ARTICLE
Journal of Cellular Biochemistry 108:1399–1409 (2009)

Journal of Cellular Biochemistry

High-Pressure Freezing of Spermiogenic Nuclei Supports a Dynamic Chromatin Model for the Histone-to-Protamine Transition

Garnet Martens,[1] Elaine C. Humphrey,[2] Lionel G. Harrison,[3†] Begonia Silva-Moreno,[4] Juan Ausió,[4] and Harold E. Kasinsky[5*]

[1] *BioImaging Facility, Department of Botany, University of British Columbia, Vancouver, British Columbia, Canada V6T 1Z4*

[2] *Advanced Microscopy Facility, University of Victoria, Victoria, British Columbia, Canada V8W 3P6*

[3] *Department of Chemistry, University of British Columbia, Vancouver, British Columbia, Canada V6T 1Z1*

[4] *Department of Biochemistry and Microbiology, University of Victoria, Victoria, British Columbia, Canada V8W 3P6*

[5] *Department of Zoology, University of British Columbia, Vancouver, British Columbia, Canada V6T 1Z4*

ABSTRACT

In this study, we present for the first time a description of the dynamic chromatin changes that occur during spermiogenesis in the internally fertilizing caenogastropod mollusc *Nucella lamellosa*. Chromatin condensation in developing sperm cells in some animals, such as the model biological system used here, involves the histone-to-protamine transition and proceeds through a patterning stage from granules to fibers to lamellae. This may be due to the physicochemical phenomenon of phase separation by spinodal decomposition, a dynamic mechanism known to generate pattern. This hypothesis is based entirely on published transmission electron microscopy photomicrographs using conventional fixation technology. We now report that spermatid nuclear patterning and subsequent condensation in testis of *Nucella lamellosa* fixed by high-pressure freezing and freeze substitution (HPF/FS) is similar to that in glutaraldehyde-fixed testis, and can be related to the processing of sperm nuclear basic proteins (SNBPs). J. Cell. Biochem. 108: 1399–1409, 2009.

KEY WORDS: SPERMIOGENESIS; CHROMATIN; NUCLEOPLASM; PATTERNING; CONDENSATION; HIGH-PRESSURE FREEZING; SPINODAL DECOMPOSITION; TRANSMISSION ELECTRON MICROSCOPY; SPERM NUCLEAR BASIC PROTEINS; *NUCELLA LAMELLOSA*

During post-meiotic spermiogenesis, a very distinctive but transient formation of pattern can occur in the developing spermatid nucleus as chromatin forms granules, then fibers, and then lamellae. This takes place before the chromatin is tightly condensed in the head of the mature sperm by an ionic crystallization as, for example, in the marine snail *Murex brandaris* [Amor and Durfort, 1990; Càceres et al., 1994, 1999, 2000].

Harrison et al. [2005] have presented a hypothesis for this transient patterning in the *M. brandaris* spermatid nucleus, as well as in an octopus and an insect, based on a dynamic mechanism known as spinodal decomposition [Cahn, 1965]. In this process there is a gradual separation between two phases, chromatin and nucleoplasm, during the initial approach of the spermatid nucleus to equilibrium [Jantzen and Herman, 1978]. In such a dynamic mechanism, pattern in the order of tens of nanometers arises from diffusive instability during the phase separation [Jones, 2002].

According to Gunton and Droz [1983, p. 5] "the initial evolution of an unstable state involves infinitesimally small long-wave fluctuations of the local order parameter (such as the local concentration). This initial process is known as spinodal decomposition and is physically manifest as a finely dispersed precipitate which gradually coarsens." It occurs "when an infinitesimal concentration fluctuation of infinite extension decreases the free energy of the system, resulting in its decomposition" [Raspaud et al., 1998, p. 385].

†Deceased March 17, 2008.

Grant sponsor: Natural Sciences and Engineering Research Council of Canada (NSERC); Grant number: OGP 0046399-02.

*Correspondence to: Dr. Harold E. Kasinsky, Department of Zoology, University of British Columbia, Vancouver, BC, Canada V6T 1Z4. E-mail: kasinsky@zoology.ubc.ca

Received 5 May 2009; Accepted 4 September 2009 • DOI 10.1002/jcb.22373 • © 2009 Wiley-Liss, Inc.
Published online 14 October 2009 in Wiley InterScience (www.interscience.wiley.com).

Spinodal decomposition occurs uniformly throughout the entire chromatin/nucleoplasm, as seen in glutaraldehyde-fixed spermatids of the marine snail *M. brandaris* and the octopus *Eledone cirrhosa* [Harrison et al., 2005]. However, in the homopteran insect *Philaenus spumarius* [Chevaillier, 1970, Figs. 2–6], electron micrographs show that there are two distinct groupings in the nucleus of the developing spermatid: patterning chromatin/nucleoplasm in the bulk of the interior of the nucleus and two ''patches'' of granular chromatin at the left and right edges of the transverse sections. Here spinodal decomposition occurs only in the bulk interior of the nucleus [Harrison et al., 2005, Figs. 1B–E and 5II].

Furthermore, spinodal decomposition differs markedly from reaction–diffusion mechanisms [Turing, 1952] that also form pattern in the order of tens of nanometers, insofar as the latter are out of equilibrium, require continuous synthesis and breakdown of the patterning substances (which is not happening to DNA during spermiogenesis) and can only form pattern rapidly in milliseconds, rather than slowly in days, as occurs in spermiogenesis.

In order to account for the possible weeks long duration of patterning during spermiogenesis, before the chromatin becomes tightly condensed, Harrison et al. [2005] have further postulated that the formation of microemulsions [Evans and Wennerstrom, 1999] might stabilize the transient pattern. Microemulsions are liquid mixtures in which suspended substances show pattern with spacing in the order of tens of nanometers, the same magnitude as patterning due to spinodal decomposition.

Such patterning of chromatin in the spermatid nucleus has heretofore been observed only by glutaraldehyde fixation (GLUT-fixed) and osmium tetroxide staining, conventional procedures for transmission electron microscopy (TEM) that have been used for the last 50 years [Afzelius and Maunsbach, 2004]. Before studying this transient patterning phenomenon any further, it is important to confirm the in situ morphology of chromatin/nucleoplasm in the developing spermatid nucleus by an independent method.

It is known that fixation by rapid high-pressure freezing and freeze substitution (HPF/FS), followed by heavy metal staining in preparation for TEM [McDonald, 1999], provides a more accurate representation of ''mottled'' chromatin structure at the primary constriction of metaphase chromosomes in vertebrate somatic PtK1 cells than does conventional procedures [McEwan et al., 1998]. We have therefore examined, for the first time, chromatin patterning during spermiogenesis in the marine snail *N. lamellosa* using both HPF/FS and GLUT-fixed procedures, and have related the observed patterning to the likely processing of the sperm nuclear basic proteins (SNBPs) present in the spermatid nucleus.

MATERIALS AND METHODS

ANIMALS

Male *N. lamellosa* (frilled dogwinkle) [Rehder, 1981, p. 527] were collected from the west coast of Vancouver Island with the assistance of the staff of the Bamfield Marine Station, BC, and transported in seawater to flow-through seawater tanks in the Department of Zoology at the University of BC in Vancouver. All animals were treated in accordance with the Guidelines of the Canadian Council on Animal Care.

TISSUE FIXATION AND TRANSMISSION ELECTRON MICROSCOPY

Five snails were removed from the seawater tanks and placed in 100 ml of 10% (w/v) $MgCl_2$ in seawater for 10 min. Such anesthetized animals were placed in a vice and their shells cracked open. The testis was removed and dissected under cooled seawater into 1 mm^3 pieces. These pieces were either placed inside type B (depth 300 μm) aluminum HPF planchettes (M. Wohlwend, Sennwald, Switzerland), which had been previously filled with either 1-hexadecane [Muller-Reichert et al., 2003], and either high-pressure frozen with a Baltec HPM010 (Liechtenstein), or chemically fixed at room temperature in 2.5% (v/v) glutaraldehyde in artificial seawater for a minimum of 1 h.

HPF samples were placed in a Leica AFS freeze substitution chamber with 1% (w/v) osmium tetroxide and 0.1% (w/v) uranyl acetate (UA) in anhydrous acetone for 4 days at −85°C, followed by a slow 12-h ramp to −20°C for 6 h and a 24-h ramp to 4°C. The substituted samples were then warmed to room temperature and rinsed in clean anhydrous acetone. The GLUT-fixed samples were stored in 4°C seawater until further processing. The samples were then fixed in 2% (w/v) osmium tetroxide in artificial seawater, rinsed with distilled water, and dehydrated from 30% (v/v) ethanol through to anhydrous 100% ethanol.

Resin infiltration for both the HPF and GLUT-fixed samples (1:1 mixture of Epon and Spurr's) was done under vacuum and microwave processed using the Pelco 3450 laboratory microwave set to 300 W [modified from Giberson and Demaree, 1999]. Samples were polymerized overnight at 60°C. Ultrathin (60 nm) sections were cut using a 35° diamond knife on a Leica Ultracut T and ribbons were collected on carbon/formvar-coated copper slot grids. After staining with 2% (w/v) UA and Sato's lead images were collected using a 1K AMT side mount camera on a Hitachi H7600 transmission electron microscope operated at 80 kV. Plates and image quality was adjusted using Photoshop CS4™.

All measurements of λ, d, w, and n.d. on TEM photomicrographs were made manually by H.E.K. using a finely calibrated Staedtler steel ruler.

SNBP PREPARATION AND FRACTIONATION

SNBPs were extracted from *N. lamellosa* testes with 0.4 N HCl using the protocols described previously [Wang and Ausió, 2001]. The HCl extracts were fractionated by reversed-phase high-performance liquid chromatography (RP-HPLC), as described elsewhere [Ausió, 1988].

SNBP CHARACTERIZATION

Acetic acid (5%)–urea (2.5 M) polyacrylamide gel electrophoresis (PAGE) analysis of SNBPs and the amino acid analysis characterization of the HPLC fractions were carried out as in Eirín-López et al. [2008] and Wang and Ausió [2001].

RESULTS

HIGH-PRESSURE FREEZING VERSUS GLUTARALDEHYDE FIXATION OF SPERMATID NUCLEI

A panoramic view in photomicrographs of a number of spermatid nuclei in *N. lamellosa* testis shows several groups of haploid

spermatids in the TEM. In each group the cells are at the same step of spermiogenesis in both GLUT-fixed (Fig. 1A,C) and HPF/FS (Fig. 1B,D) tubules.

Sperm nuclei in transverse section with highly condensed chromatin are visible as a group in the upper left (Fig. 1A) and lower right corner (Fig. 1C) of GLUT-fixed tubules, as well as in a group in the lower right of a tubule prepared by HPF/FS (Fig. 1B,D). Mature sperm heads are elongated (Fig. 1E), as in the congeneric species *Nucella lapillus*, where the ''sperm head consists of a cylinder of nuclear material which encloses the anterior portion of the flagellar shaft'' [Walker and MacGregor, 1968, p. 99]. The *N. lamellosa* sperm nuclei seen in Figure 1A–D are present in the later ''condensation'' stage of spermiogenesis [Harrison et al., 2005].

Mid-spermatid nuclei that display a distinct lamellar pattern of chromatin/nucleoplasm condensation are visible in both a GLUT-fixed tubule (Fig. 1C, middle) and a tubule prepared by HPF/FS

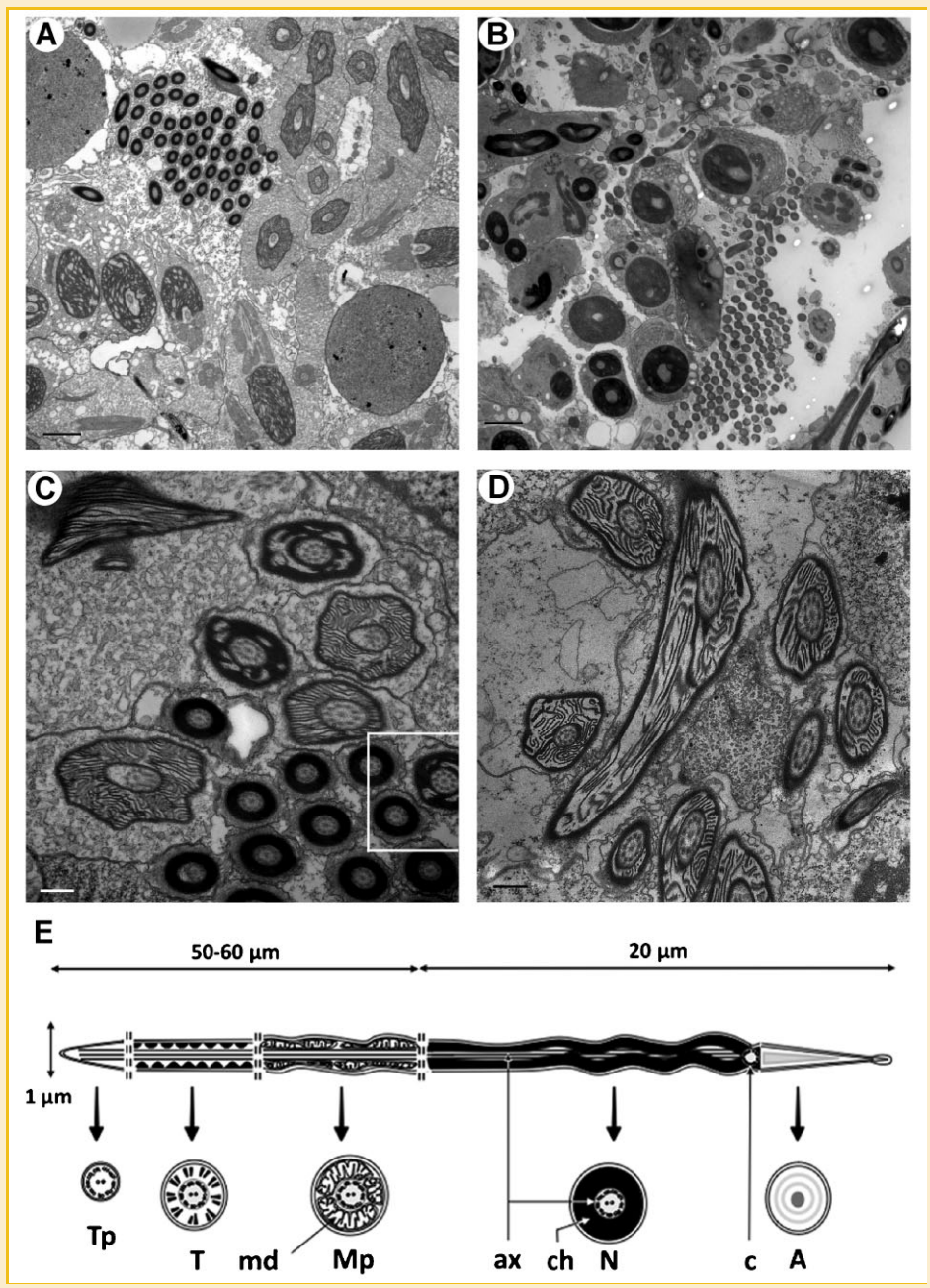

Fig. 1. Panoramic view of spermatid nuclei in *N. lamellosa* testis. A,C: GLUT-fixed tubules. B,D: HPF/FS tubules. White boundary lines in C, lower right indicate the region of the GLUT-fixed testis shown in greater detail in Figure 6E. Bars: (A,B) 2 μm; (C,D) 0.5 μm. (E) Diagram illustrating the structure of a portion of the tubular nucleus (19 μm, total length) and the acrosome (1 μm) in the mature sperm head of HPF/FS fixed *N. lamellosa* testis, with the flagellar axoneme deeply penetrating the nucleus. Chromatin is homogeneously condensed in this internally fertilizing sperm, as indicated in both longitudinal (top) and transverse (bottom) views. A, acrosome; ax, axoneme; c, centriole; ch, chromatin; md, mitochondrial derivative; Mp, middle piece; T, tail; Tp, terminal piece.

(Fig. 1D, middle). Such spermatid nuclei are present in the earlier "patterning" stage of spermiogenesis [Harrison et al., 2005].

In order to observe the development of the post-meiotic spermatid nucleus in its progressive sequence towards a complex lamellar pattern and subsequently to final chromatin condensation, we compare TEM photomicrographs from HPF/FS tubules (Fig. 2, steps A–E) and GLUT-fixed tubules (Fig. 2, steps F–J). The TEM photomicrographs in these sequences are all displayed at the same magnification, since the volume of the nucleus progressively decreases during spermiogenesis.

It is apparent that HPF/FS steps A–D have a more rounded nuclear membrane than the slightly ragged nuclear membranes in GLUT-fixed steps F and G, and the much more ragged nuclear membranes in GLUT-fixed steps H and I. However, features of the chromatin and nucleoplasm in the developing spermatids appear to be similar in both fixation procedures.

Interestingly, both HPF-FS steps B and C and GLUT-fixed steps G and I are slightly oblique in Figure 2, due to the fact that the spermatid nucleus twists at these steps of spermiogenesis. A similar twisting has been observed by Walker and MacGregor [1968] and Walker [1970] in GLUT-fixed spermatids of the congeneric species *N. lapillus*, corresponding to HPF/FS step C in *N. lamellosa* (Fig. 2).

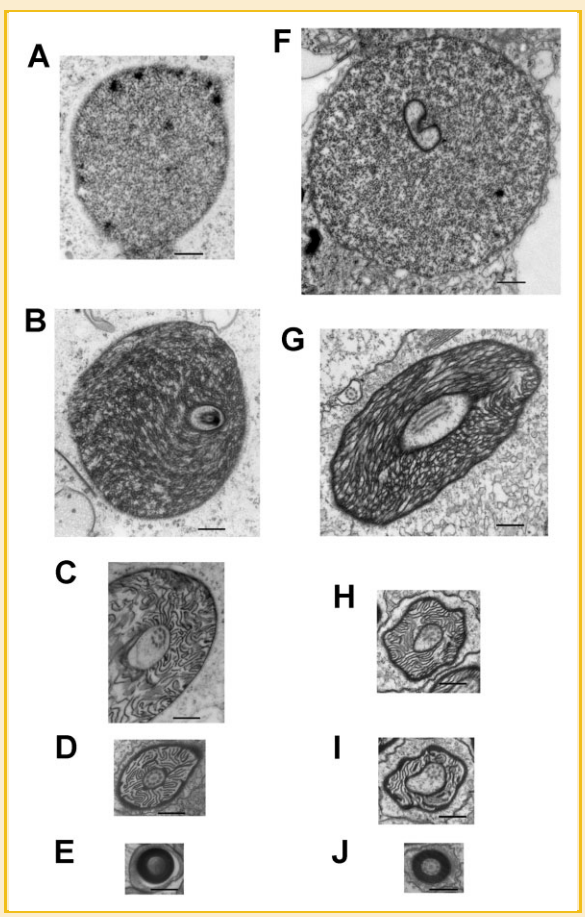

Fig. 2. TEM photomicrographs showing steps in the patterning and condensation sequence within a developing spermatid nucleus of *N. lamellosa*. HPF/FS: steps A–E; GLUT-fixed: steps F–J. Sections are slightly oblique in steps B, C, G, and I and transverse in steps D, E, H, and J. Bars: 500 nm.

TEM EVIDENCE FOR CHROMATIN PATTERNING BY SPINODAL DECOMPOSITION

There are four characteristic features of spermiogenesis seen in these TEM photomicrographs for *N. lamellosa* that, taken together, provide fairly strong evidence that the complex pattern formation seen in both HPF/FS and GLUT-fixed developing spermatid nuclei is due to the thermodynamics of phase separation by spinodal decomposition, based on diffusive mobility in the approach towards chemical equilibrium [Harrison et al., 2005].

Morphological Development. First, the sequence during spermiogenesis, from granules with diffuse boundaries to fibers to lamellae with sharp boundaries, observed by TEM photomicrographs (Fig. 2) both in HPF/FS steps A–C and GLUT-fixed steps F–H, generally resembles the formation of lamellae-like pattern in the "coarsening" of iron–aluminum alloys after a cold quench from high temperatures [Oki et al., 1977]. Since the "morphology of either isothermal spinodal decomposition or spinodal decomposition during continuous cooling are the same" [Jantzen and Herman, 1978, p. 144], we may compare patterning in a cellular system with that in a non-cellular system. In both instances, the interface between phases starts off being very diffuse but sharpens by the lamellar phase [Cahn and Charles, 1965].

Perpendicularity. Secondly, all lamellae run either perpendicularly into the boundary of the nucleus or the flagellar shaft in transverse sections or parallel to the nuclear envelope or flagellar shaft in longitudinal sections.

This phenomenon occurs at the nuclear envelope during the patterning stage of spermiogenesis in both HPF/FS (Figs. 1D and 2C) and GLUT-fixed (Figs. 1C and 2H) spermatids, as well as at the membrane bordering the flagellar shaft (GLUT-fixed: Figs. 1C and 2H; HPF/FS: Figs. 1D, 2C, and 5A). This is because there is a barrier to diffusion at these membranes as they are at the boundary of a patterning system where the concentration profile is flat [Harrison, 1993].

Spinodal decomposition can occur because a very tiny change of concentration initiates a sinusoidal concentration wave which has a diffusion rate of 0 at both the boundary of the nuclear envelope and the boundary of the flagellum; hence, the concentration gradients are 0 at these locations in the spermatid nucleus [Harrison et al., 2005, Fig. 7].

Furthermore, the amplitude of this sinusoidal concentration wave can grow, but only for a small range of wavelengths. This is the "essence of the ability to form pattern" [Harrison et al., 2005, p. 84 and Fig. 8] and "in the absence of any observable strong interaction between intranuclear chromatin and any component of the nuclear surface, there seems to be no very probable structural reason why lamellae should line up *perpendicular* to the nuclear boundary" [Harrison et al., 2005, p. 85, italics in original].

As is the case with the marine snail *M. brandaris* [Harrison et al., 2005, Fig. 9], this is fairly strong evidence for dynamic patterning involving diffusion.

Bicontinuity. Thirdly, in the patterning steps of spermiogenesis for HPF/FS spermatids (Figs. 1D, 2C, and 5A) and GLUT-fixed spermatids (Figs. 1C and 2H), the electron dense chromatin and the clear nucleoplasm each appears to be continuous, rather than as one continuous phase and one disperse phase.

Such bicontinuity [Harrison et al., 2005], also referred to as "interconnectivity" [Gunton and Droz, 1983, p. 5] or "mutual connectivity" [Jantzen and Herman, 1978, p. 143], is a feature that can be seen in colloidal microemulsions *at* thermodynamic equilibrium [Bodet et al., 1988], as well as during spinodal decomposition in the dynamics of the *approach to* equilibrium. According to Jones [2002, p. 150]: "Complex bicontinuous phases are probably best thought of as structures that arise from the distortion of a lamellar phase. This distortion is topological in nature, because the resulting phases have quite different connectivities to the lamellar phase."

Constancy of λ_m. Fourthly, it is apparent in Figure 2 that there is a constancy of spacing between nearest neighbor chromatin structures during the patterning stage of steps A–C in HPF/FS tubules and steps F–H in GLUT-fixed tubules. This gives way to the condensation of chromatin in the final steps D, E, and I, J, respectively (Fig. 2.) Constancy of spacing during the patterning stage is characteristic of the gradual increase of inhomogeneity that occurs during spinodal decomposition [Jones, 2002; Harrison et al., 2005].

The TEMs in the developmental sequences in Figure 2 are all displayed at the same magnification. This is done in order to highlight the constancy of the pattern repeat distance between the middle of one dark chromatin stripe (or dot), across the nucleoplasm, to the middle of the neighboring chromatin stripe (or dot) within a spermatid nucleus during the patterning and condensation stages (Fig. 3). This spacing, called λ (lambda), is the pattern repeat distance and was measured directly on the printed TEM micrographs using a finely calibrated steel ruler.

According to the thermodynamics of spinodal decomposition [Cahn, 1965], a spatially uniform state forms a pattern by diffusive instability which, for maximum growth rate, shows a dominant pattern repeat distance, called λ_m, corresponding to the maximum growth rate constant k_g [Harrison et al., 2005, Fig. 8B].

In fact, Figure 4 indicates that λ_m shows a similar constancy of spacing from either 35–40 nm (step A, HPF/FS) or 30–35 nm (step F, GLUT-fixed) in granules to 45–50 nm in lamellae during the patterning stage in both HPF/FS (step C) and GLUT-fixed (step H) spermatid nuclei. This is followed by a dramatic drop of λ_m to 10–15 nm in the condensation stage (Fig. 4, step D or I, respectively), in agreement with the visual impression from the TEM photomicrographs in Figure 2. A similar constancy of λ_m from 20–25 nm in granules to 30–35 nm in lamellae during the patterning stage has been observed previously [Harrison et al., 2005, Fig. 5III] in the GLUT-fixed spermatid nuclei of another muricid caenogastropod [Pechenik, 2005, p. 272] *M. brandaris*. In this case, the constancy of spacing in HPF/FS spermatid nuclei is more pronounced than in GLUT-fixed *N. lamellosa*.

At the end of the patterning stage, the lamellae that are perpendicular to the nuclear envelope and the flagellar shaft (HPF/FS: Figs. 1D, 2C, and 5A; GLUT-fixed: Figs. 1C and 2H) now become stacked parallel to the envelope and the shaft in both HPF/FS (Figs. 5B and 6C,D) and GLUT-fixed (Fig. 6E, right) spermatid nuclei. Finally, a homogeneously condensed nucleus is formed in the mature sperm (HPF/FS: Fig. 2E; GLUT-fixed: Fig. 1C, lower right; Fig. 2J; Fig. 6E, left). This condensation process has been visualized in a very dramatic fashion by the wave-like chromatin fibers (Fig. 6A) in HPF/FS spermatid nuclei that are forming stacked lamellae at the boundary of both the nucleus and the flagellar shaft (Figs. 5B and 6A,B).

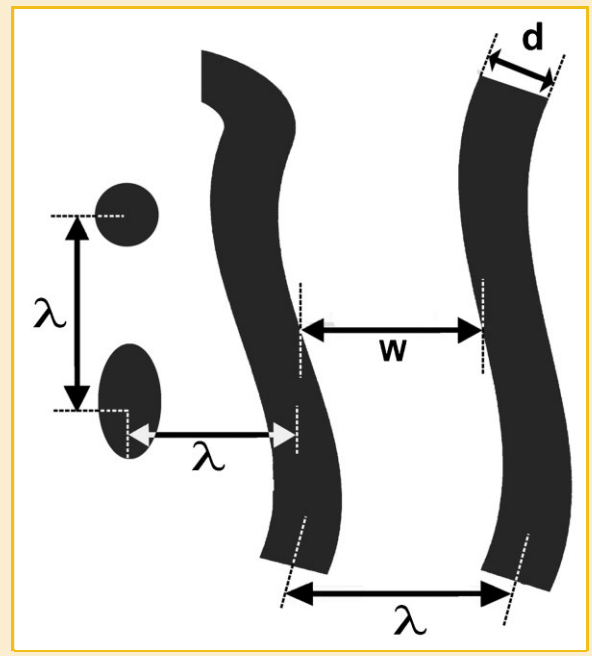

Fig. 3. Measurements of chromatin/nucleoplasm pattern in TEM photomicrographs of the spermatid nucleus: λ, pattern repeat distance, from the middle of a chromatin fiber (undulating gray stripe or gray dot), across the nucleoplasm (white) to the middle of another chromatin fiber; d, diameter of chromatin fiber; w, width of nucleoplasm [based on Harrison et al., 2005, Fig. 4].

ELECTROPHORETIC AND AMINO ACID ANALYSIS OF SNBPS IN *N. LAMELLOSA*

What changes in the concentration or type of SNBP could account for the transition from constant-λ patterning to shrinking-λ condensation in *N. lamellosa*? Analysis of SNBPs in the nucleus of *N. lamellosa* spermatids indicates that proteolytic processing of a protamine precursor and dephosphorylation of its serine/threonine residues are possible candidates.

A representative electrophoretic pattern of the SNBPs from an HCl extract of the testes of *N. lamellosa* is shown in Figure 7A. As can be seen (lanes 3 and 4), the SNBPs exhibit a heterogeneous composition in which somatic-like histones co-exist with a complex mixture of protamine precursors (Nl1–3) that have an intermediate mobility between histones and vertebrate protamines. The complexity of the electrophoretic bands is the result of the heterogeneous cell composition of the testes chosen for this analysis and reflects the

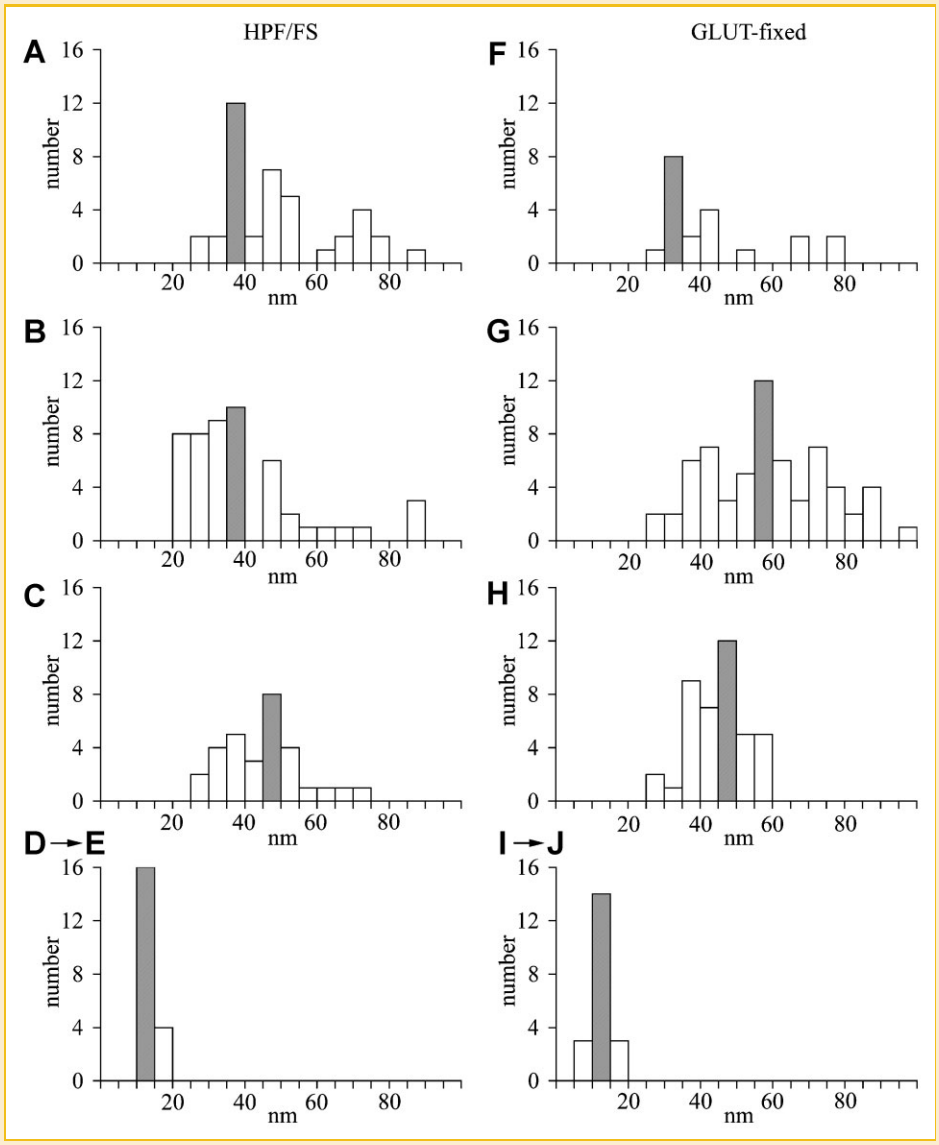

Fig. 4. Histograms of λ values for spermatid nuclei in TEM micrographs of HPF/FS steps A–C (Fig. 2) and D, E (Fig. 6D), as well as GLUT-fixed steps F–H (Fig. 2) and I, J (Fig. 6E, upper right). The vertical axis indicates the number of measurements. All bars are for 5 nm intervals. Cross-hatching shows the dominant spacing (λ_m) for each step in the patterning and condensation stages of spermiogenesis. Twenty to 60 measurements were made manually for each step in order to obtain a fair choice of details to measure based on their prevalence in the patterns.

cellular heterogeneity that occurs in the electron micrographs (Figs. 1 and 2).

Figure 7B shows a reversed-phase HPLC elution profile obtained with such a SNBP mixture, and Table I provides the amino acid composition of the protamine precursor proteins purified in this way. The comparison of the amino acid composition of the Nl1–3 fractions in *N. lamellosa* to that of SNBP fractions from closely related caenogastropod species within the same muricid family [Pechenik, 2005, p. 272]; namely, Tx1, Tx3, and TxP in *Thais xocolata* [Ribes et al., 2001] and Mb1, Mb3, and MbP in *M. brandaris* [Càceres et al., 1994], suggests that the Nl1–3 proteins correspond to protamine precursors present in spermatids with different extents of maturity.

In addition, the presence of both serine and threonine residues in Nl1–3 protamine precursors (Table I) suggests that phosphorylation/dephosphorylation sites are available for covalent modification in *N. lamellosa* during spermiogenesis, whereas only serine residues are present in the mature protamine of sperm in *T. xocolata* and *M. brandaris* due to removal of threonine residues by proteolytic processing [Càceres et al., 1999, 2000].

DISCUSSION

SPERMIOGENIC CHROMATIN PATTERNING BY SPINODAL DECOMPOSITION: AN HYPOTHESIS

HPF/FS preparation of testis from the caenogastropod *N. lamellosa* yields TEM photomicrographs (Fig. 2) that, for the first time, validate the data from corresponding GLUT-fixed testes showing chromatin patterning and condensation during spermiogenesis. Harrison et al.

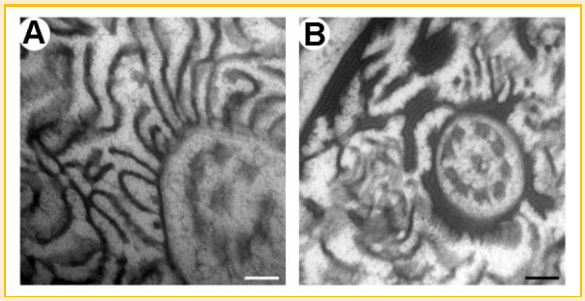

Fig. 5. *N. lamellosa* spermatids (HPF/FS) showing the developmental progression of the nucleus during spermiogenesis from (A) the patterning step (transverse section), where lamellae run into the boundary of the flagella shaft in a perpendicular manner, to (B) the condensation step (transverse section), where lamellae are arranged in parallel stacks at both the nuclear envelope (upper left) and the boundary of the flagella shaft (lower right). Both cells are from the same tissue. Bars: 100 nm.

[2005] have postulated that the coarsening pattern in GLUT-fixed testis from another muricid caenogastropod, *M. brandaris*, developing from diffuse granules to fibers to sharp lamellae, can be explained as a phase separation of liquids due to spinodal decomposition, with subsequent stabilization of the transient patterning by microemulsification.

This is also apparent in HPF/FS, as well as GLUT-fixed, spermatids of *N. lamellosa*, as TEMs display not only the feature of coarsening but also the constancy of λ_m, perpendicularity and bicontinuity of chromatin/nucleoplasm that are characteristic of spinodal decomposition during the patterning stage. In addition, the formation of wave-like chromatin bundles (Fig. 6A,B) in the transition to the condensation stage in HPF/FS spermatids demonstrates dramatically the motility of chromatin/nucleoplasm during spermiogenesis.

Thus, during the patterning stage in HPF/FS spermatid nuclei of *N. lamellosa* (Fig. 2, left column), the nuclear diameter decreases from 3.3 to 3.1 μm and 2.5 μm (Fig. 8, steps A–C), then from 1.8 μm in the subsequent condensing stage to 0.7 μm in mature sperm with homogeneous chromatin (Fig. 8, steps D and E). Correspondingly, in GLUT-fixed spermatids (Fig. 2, right column), the nuclear diameter decreases from 4.4 to 2.5 μm and1.6 μm in the patterning stage (Fig. 2, steps F–H), then from 1.5 μm in the following condensing stage to 0.6 μm in mature sperm with homogeneous chromatin (Fig. 2, steps I and J).

As the nuclear volume decreases progressively, λ_m remains constant during the patterning stage in the range of 35–50 nm in HPF/FS spermatids (Fig. 4, steps A–C) and from 30 to 60 nm in GLUT-fixed spermatids (Fig. 4, steps F–H), with both fixation methods showing the same λ_m of 45–50 nm in the corresponding lamellar steps (Fig. 4, steps C and H).

Again, in both cases, λ_m decreases from 45–50 nm (Fig. 4, steps D and I) to the same λ_m of 10–15 nm during the condensation stage (Fig. 6D,E). Since both fixation methods yield such similar results, this is fairly strong evidence for the occurrence of phase separation by spinodal decomposition during the patterning stage of spermiogenesis.

During the patterning stage and the beginning of condensation, the average diameter (d_{avg}) of the chromatin fiber ranges from 15 to 19 nm in HPF/FS spermatids (Fig. 8, steps A–D; based on 20 measurements), falling to 6 nm during the condensation stage (Fig. 6D), and similarly 16–18 nm for GLUT-fixed spermatids (Fig. 2, F–H) falling to 8 nm (Fig. 6E, right).

Also, the average width (w_{avg}) of the nucleoplasm is quite similar in spermatids fixed by each of these procedures, ranging from 21 to 33 nm during patterning and the beginning of condensation in HPF/FS spermatids (based on 20 measurements, in Fig. 8, steps A–C), or 27–37 nm in GLUT-fixed spermatids, and falling during condensation to 9 nm (HPF/FS) or 5 nm (GLUT-fixed).

Taken together, the congruence of results for λ_m, d_{avg}, and w_{avg} by both fixation methods tells us that we can now reliably examine the literature over the past half century [Afzelius and Maunsbach, 2004], which is based on GLUT-fixed methodologies, in order to reveal what other animals may show chromatin patterning during spermiogenesis due to phase separation by spinodal decomposition.

For example, one finds similar morphological development of chromatin patterning, perpendicularity of chromatin to nuclear boundaries and bicontinuity of the chromatin and nucleoplasm phases in GLUT-fixed testes of other internally fertilizing caenogastropods in the family Muricidae, such as *N. lapillus* [Walker and MacGregor, 1968; Walker, 1970], *N. crassilabrum* [Gallardo and Garrido, 1989], *Chorus giganteus* [Jaramillo et al., 1986], and *M. brandaris* [Harrison et al., 2005]. In addition, *N. crassilabrum* and *C. giganteus* have the same $\lambda_m = 45–50$ nm in their step C of spermiogenesis as in GLUT-fixed (and HPF/FS) *N. lamellosa*. This value is somewhat lower in *M. brandaris* ($\lambda_m = 30–35$ nm) and *N. lapillus* ($\lambda_m = 20–25$ nm), but still within the range of tens of nanometers expected for phase separation by spinodal decomposition.

THE HISTONE-TO-PROTAMINE TRANSITION AND SPINODAL DECOMPOSITION

What initiates spinodal decomposition in the patterning stage of spermiogenesis in *N. lamellosa* and what causes the transition to the condensation stage? Like the classical spinodal decomposition that is induced experimentally by a rapid cold quench into a very hot mixture of sodium oxide–silicon dioxide glass [Cahn and Charles, 1965] or an iron–aluminum alloy [Oki et al., 1977], such a type of phase separation in a spermatid nucleus forms a transient pattern that is observable by TEM.

However, for spermatid nuclei, this occurs isothermally in a living cell. Raspaud et al. [1998] have successfully used spinodal decomposition theory to account for the experimental observations of double-stranded DNA precipitation in vitro by different concentrations of polyamines at room temperature and pH 7.6, but they did not use TEM to observe the precipitation process.

In the case of spermiogenesis, where the nuclear volume progressively decreases over a period of several weeks [Harrison et al., 2005], we propose that the histone-to-protamine replacement during the patterning stage acts in place of a cold quench of inanimate materials.

For example, the entry of protamine precursor (Pp) into the *N. lamellosa* HPF/FS (or GLUT-fixed) spermatid nucleus (Fig. 8), while histones in the chromatin are being acetylated, may allow for the separation of two phases by "gradual development of patterned

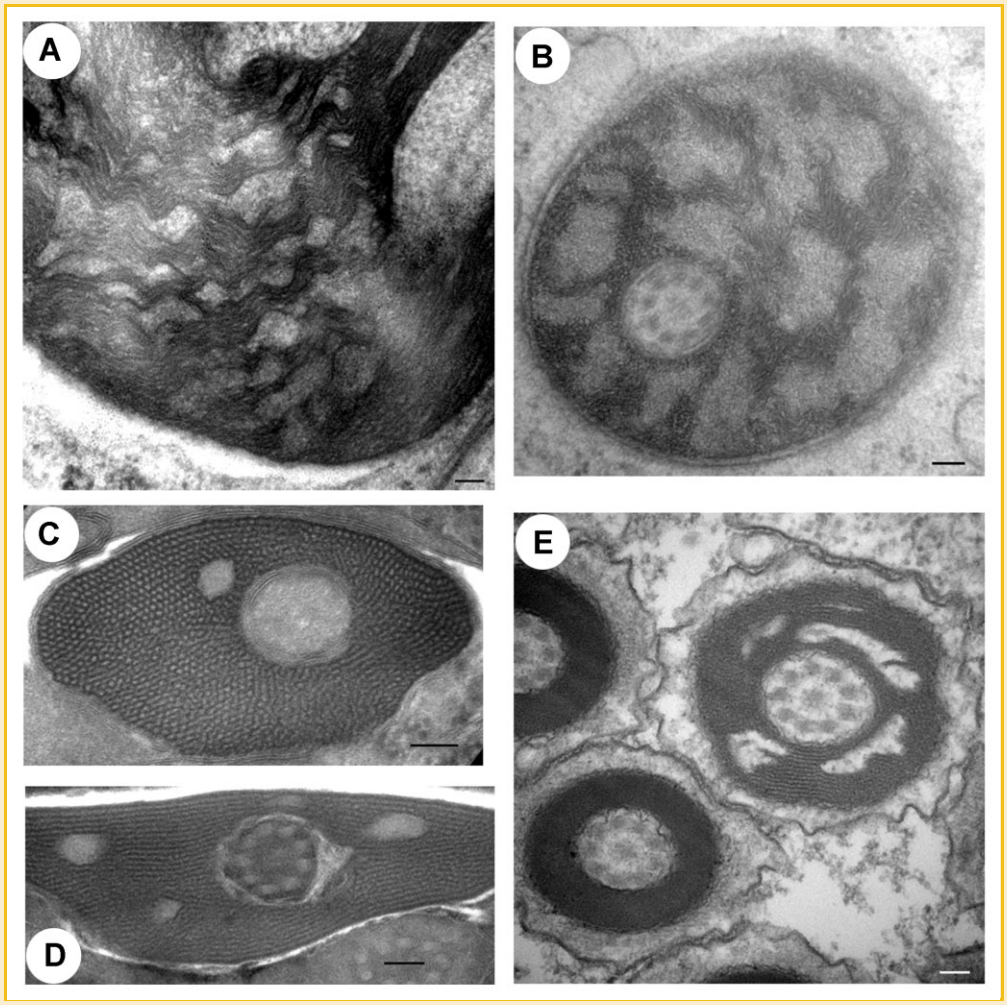

Fig. 6. *N. lamellosa* spermatid nuclei showing the developmental progression from stacked lamellae to homogeneously condensed chromatin during the condensation stage of spermiogenesis. A: HPF/FS. Wave-like pattern of chromatin fibers in the nucleus at the beginning of the condensation stage (slightly oblique section), forming stacked lamellae at the boundaries of the nucleus (lower center) and flagellar shaft (upper right). B: Global view (HPF/FS; transverse section) of the nucleus showing stacked lamellae as in (A) in distinct regions of the nucleus. C,D: Nuclei (HPF/FS; transverse sections) showing stacking of lamellae during the latter part of the condensation stage [35 lamellae are present in (C) and 30 lamellae in (D)]. E: Nuclei (GLUT-fixed; transverse sections) with a progression from stacked lamellae (right: 14 lamellae), to homogeneous chromatin (left). All cells are from the same tissue. See white boundary lines in Figure 1C (lower right) to locate these three nuclei in relation to other spermatid nuclei in the same section that are in the earlier patterning stage. Bars: 100 nm.

concentration changes'' [Harrison et al., 2005, p. 88]. This does appear to occur during spermiogenesis in another mollusc, the cephalopod cuttlefish *Sepia officinalis* [Kurtz et al., 2007]. Subsequently, removal of acetylated histones and proteolytic processing of the protamine precursor, along with the dephosphorylation of its serine or threonine residues [Càceres et al., 1994, 1999], might initiate the transition from the constant-λ patterning stage to the shrinking-λ condensation stage in *N. lamellosa*.

Harrison et al. [2005, p. 86] have pointed out the following: ''Timing of chemical changes is also relevant to the possibility that the patterned systems are microemulsions. An emulsion consists of two phases with geometries constrained by the nature of the interface between them. This requires, a substance, the emulsifying agent, preferentially attracted to that interface, perhaps a *protamine* [italics added].'' It therefore follows that: ''Spinodal decomposition gives the dynamics while microemulsion formation gives stability to phases separated in a patterned way on a scale of tens of nanometers.''

We now argue that in the case of *N. lamellosa* and other muricid snails, the emulsifying agent may be *pro-protamine* rather than mature protamine. The electrophoretic and chromatographic results (Fig. 7), as well as the amino acid analysis (Table I) of SNBPs in *N. lamellosa* spermatids indicate that proteolytic processing of a protamine precursor may indeed take place during spermiogenesis. This likely occurs as well in the closely related internally fertilizing caenogastropods *T. xocolata* [Ribes et al., 2001] and *M. brandaris* [Càceres et al., 1994, 1999, 2000], both from the same family Muricidae that includes *N. lamellosa* [Ruppert and Barnes, 1994, p. 488].

Càceres et al. [1999, p. 649] point out that protein precursors in *M. brandaris* ''are subjected to a substantial number of small N-terminal deletions that gradually modify their overall charge.''

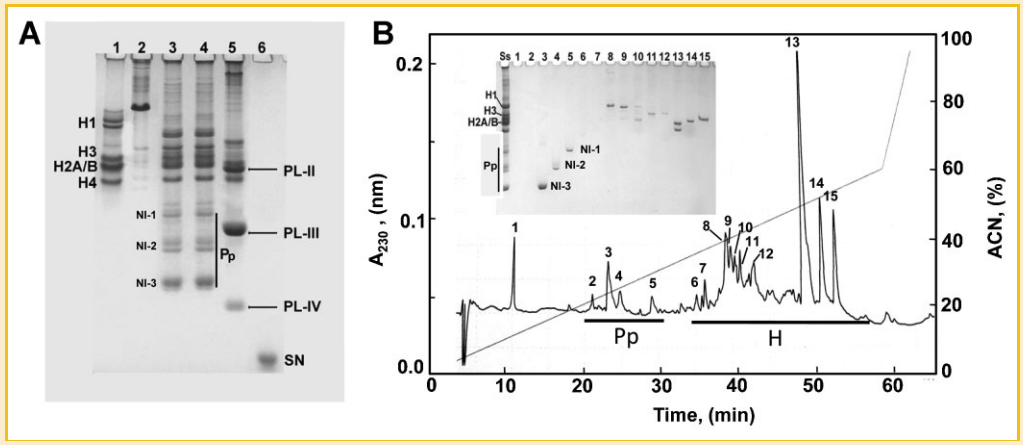

Fig. 7. HPLC and PAGE of SNBPs of *N. lamellosa*. A: Acetic acid (5%)–urea (2.5 M) PAGE of SNBPs from a testis-HCl extract of *N. lamellosa* (lanes 3 and 4) in comparison to the SNBPs of other molluscs: *Chlamys hastata* (swimming scallop, lane 1), *Spisula solidissima* (surf clam, lane 2), *Mytilus californianus* (California mussel, lane 5), and the protamine salmine (SN) from the mature sperm of salmon (*Oncorhynchus keta*, lane 6). PL-II, PL-III, and PL-IV indicate the protamine-like proteins of the sperm of *M. californianus* [Mogensen et al., 1991]. Electrophoresis is from top to bottom. B: Reversed-phase HPLC of the SNBPs of *N. lamellosa* shown in lanes 3 and 4 of (A). The inset shows the acetic acid–urea PAGE of the fractions indicated in the elution profile. A_{230}, absorbance at 230 nm; ACN, acetonitrile; H, histones; H1, H2A/B, H3, H4, individual histones; Pp, protamine precursor; SN, salmine; Ss, starting sample.

The precursor sequence in the original pro-protamine [Càceres et al., 1999, p. 655] "is made up of 35 amino acid residues of which nine are basic (five Arg, three Lys, and one His) and seven are acidic (two Asp and five Glu, four of them in a row, Glu_4)" and may "interact with both DNA and basic proteins (histones or protamines)," especially "by means of its clusters of acidic residues." Accordingly, the "successive deletions of the precursor peptide . . . might modulate the interactions of the proteins with DNA and might also be instrumental in the structural transitions undergone by the spermiogenic chromatin."

As to a possible role for dephosphorylation of serine and threonine residues in *N. lamellosa* (Table I), the single serine residue in *M. brandaris* "appears phosphorylated throughout the processing of the molecule . . . undergoing dephosphorylation only in the fully ripe spermiogenic nuclei" [Càceres et al., 1999, p. 655]. Consequently, the role of dephosphorylation is "most probably restricted to the final step of chromatin condensation (coalescence of lamellae)."

Interestingly, when the amino acid compositions of SNBPs in Table I from internally fertilizing *N. lamellosa* are compared to that of an analog PL-III SNBP from the externally fertilizing bivalve mollusc *Mytilus californiensis* [Mogensen et al., 1991], which does not pass through a patterning stage during spermiogenesis that includes a lamellar chromatin/nucleoplasm step

TABLE I. Amino Acid Composition (mol %) of the SNBPs of *Nucella lamellosa* (Nl) in Comparison to the Intermediate Protamines (1 and 3) and the Protamine (P) From *Thais xocolata* (Tx)* and *Murex brandaris* (Mb),** As Well As PL-III From *Mytilus californianus****

Amino acid	Tx1	Mb1	Tx3	Mb3	TxP	MbP	Nl-1	Nl-2	Nl-3	PL-III
Lysine	18.0	18.0	27.0	31.2	30.5	30.2	8.1	7.1	15.8	20.5
Histidine	1.0	1.2	0.7	–	–	–	1.8	1.5	0.8	–
Arginine	21.0	17.3	30.5	26.9	40.4	35.0	17.5	17.7	34.2	32.1
Aspartic acid	5.2	5.5	1.9	2.0	tr	–	10.4	8.2	4.6	–
Threonine	2.6	3.7	1.4	1.3	–	–	3.9	3.7	1.7	2.5
Serine	5.9	4.9	3.9	4.4	2.7	1.5	4.5	4.9	2.6	15.4
Glutamic acid	6.8	6.6	4.6	4.0	0.5	–	9.4	8.03	3.0	–
Proline	2.6	4.0	1.9	0.3	–	–	4.1	3.2	1.4	5.1
Glycine	16.6	16.4	22.8	23.5	25.0	31.3	18.5	26.4	27.4	7.5
Alanine	6.7	6.9	1.8	3.4	0.6	0.2	4.8	5.2	2.3	15.9
Cysteine	tr	tr	tr	0.3	tr	tr	–	–	–	–
Valine	3.1	3.4	0.9	1.0	–	–	4.1	3.2	1.7	1.1
Methionine	1.1	0.5	–	–	–	–	0.7	0.7	0.3	–
Isoleucine	3.0	3.8	tr	–	–	–	3.7	1.8	0.8	–
Leucine	4.6	5.8	1.1	1.0	–	–	2.1	3.8	1.5	–
Tyrosine	0.5	–	–		–	–	3.0	2.5	1.1	–
Phenylalanine	1.3	1.8	1.5	0.7	–	–	3.5	2.2	1.0	–
Lys + arg	39.8	35.3	57.5	58.1	70.9	65.2	25.6	24.8	50.0	52.6
Lys + arg + gly	56.5	51.7	80.3	81.6	95.9	96.6	44.1	51.2	77.4	60.1

tr, trace; lys, lysine; arg, arginine; gly, glycine.
*Ribes et al. [2001].
**Càceres et al. [1994].
***Mogensen et al. [1991].

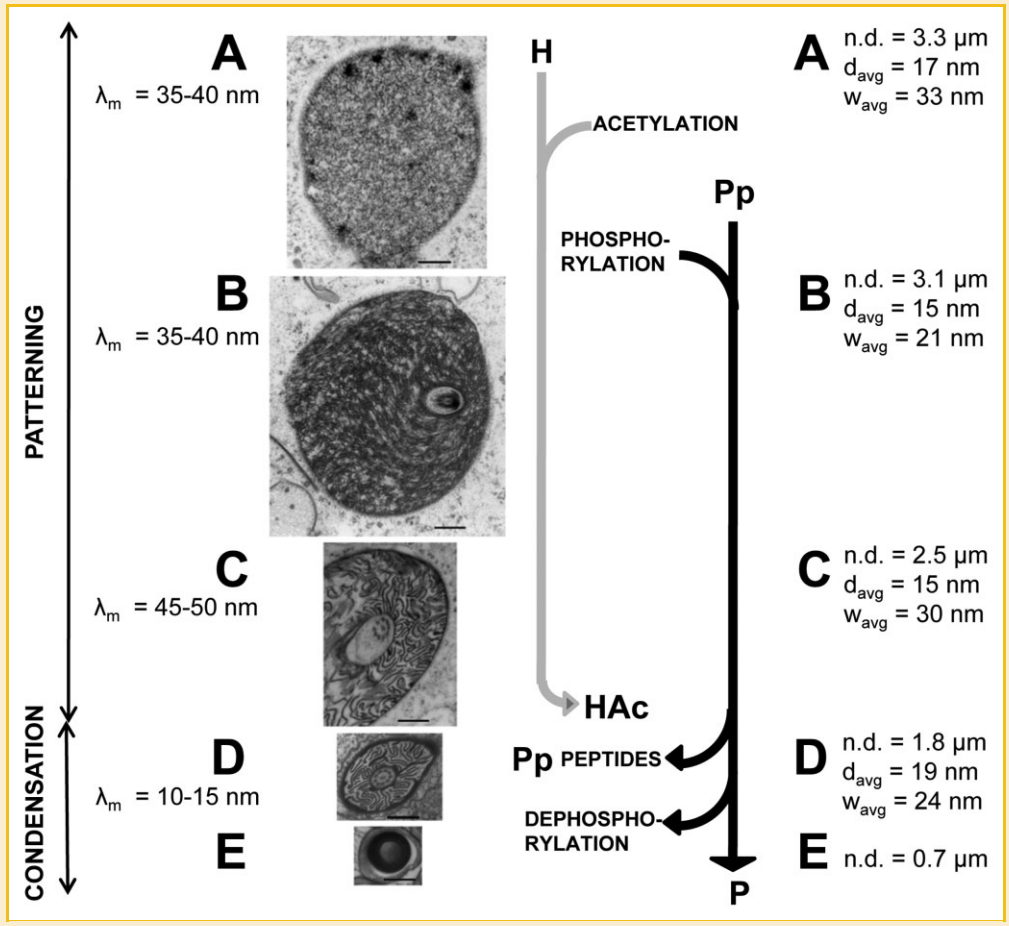

Fig. 8. Proposed correlation in the developing HPF/FS spermatid nucleus of *N. lamellosa* between pattern formation due to spinodal decomposition, a physicochemical phenomenon, and the concomitant modification and processing of histones and SNBPs. λ_m = dominant pattern repeat distance (see Fig. 4 for values) corresponding to the maximum growth rate constant k_g [Cahn, 1965; Harrison et al., 2005]. H, histones; Pp, protamine precursor; n.d., nucleus diameter (single measurement); d_{avg}, average diameter of chromatin fibers (from 20 measurements); w_{avg}, average width of nucleoplasm (from 20 measurements). Bars: 500 nm.

[Longo and Dornfeld, 1967], the basic amino acid composition (lysine + arginine) is very similar: although, in this latter instance, the mature sperm consists of a heterogeneous mixture of histone H1-related SNBPs (Fig. 7A, lane 5).

The same is also true in the case of another externally fertilizing bivalve mollusc, *Spisula solidissima*, which only contains a PL-I protein in its mature sperm (Fig. 7A, lane 2) and also does not exhibit a lamellar chromatin/nucleoplasm step during spermiogenesis [Longo and Anderson, 1969]. The main compositional difference between the proteins of these different groups appears to be the high alanine and serine content of the bivalve PLs that contrasts with the high glycine content of the caenogastropod SNBPs (Table I).

Nevertheless, a direct comparison between the two groups is not possible as, in contrast to the internally fertilizing caenogastropods, externally fertilizing bivalve molluscs retain a significant fraction (20–30%) of the somatic-like histones in their mature sperm [Avramova et al., 1984; Ausió and van Holde, 1987], whose contribution to the different chromatin/nucleoplasm transitions observed during spermiogenesis is currently unknown.

Finally, it will be interesting to extend this analysis of patterning and condensation to insect spermatid nuclei [Harrison et al., 2005], as well as to other invertebrates and vertebrates. This may assist us in bringing together the physical phenomenon of spinodal decomposition, as observed by TEM during spermiogenesis, and the biochemical data on the histone-to-protamine replacement, in order to explain the morphological development of spermiogenic chromatin/nucleoplasm in internally fertilizing animals.

ACKNOWLEDGMENTS

We gratefully acknowledge the assistance of Dr. Thomas Carefoot and the Director and staff of the Bamfield Marine Sciences Centre for helping us to obtain male specimens of *N. lamellosa*. In addition, Sandra Millen generously provided us the use of her flow-through seawater facility. We also thank Dr. Manel Chiva, Dr. Thurston Lacalli, Ellen Rosenberg, and Dr. Wayne Vogl for helpful discussions. H.E.K. wishes to thank Dr. William Milsom for providing office space during the course of this study and Alistair Blachford, Peter Judd, and Sanja LeBlanc for their computer assistance. Dr. Lionel Harrison, our coauthor and pioneer in the field of the kinetic approach to pattern formation in morphogenesis, originated the present study but, to our deep regret,

succumbed to his longstanding illness before seeing this paper to publication. We would also like to acknowledge the late Dr. Lluis Cornudella, whose earlier work with the Barcelona group on spermiogenesis in *M. brandaris* was very helpful to us. This work was supported by Natural Sciences and Engineering Research Council of Canada (NSERC) to J.A. (OGP 0046399-02).

REFERENCES

Afzelius BA, Maunsbach AB. 2004. Biological ultrastructure research; the first 50 years. Tissue Cell 36:83–94.

Amor MJ, Durfort M. 1990. Changes in nuclear structure during eupyrene spermatogenesis in *Murex brandaris*. Mol Reprod Dev 25:348–356.

Ausió J. 1988. An unusual cysteine-containing histone H1-like protein and two protamine-like proteins are the major nuclear proteins of the sperm of the bivalve mollusc *Macoma nasuta*. J Biol Chem 263:10141–11015.

Ausió J, van Holde KE. 1987. A dual chromatin organization in the sperm of the bivalve mollusc *Spisula solidissima*. Eur J Biochem 165:363–371.

Avramova Z, Zalensky A, Tsanev R. 1984. Biochemical and ultrastructural study of the sperm chromatin from *Mytilus galloprovincialis*. Exp Cell Res 152:231–239.

Bodet J-F, Bellare JR, Davis HT, Scriven LE, Miller WG. 1988. Fluid microstructure transition from globular to bicontinuous in midrange microemulsion. J Phys Chem 92:1898–1902.

Càceres C, Ribes E, Muller S, Cornudella L, Chiva M. 1994. Characterization of chromatin-condensing proteins during spermiogenesis in a neogastropod mollusk (*Murex brandaris*). Mol Reprod Dev 38:440–452.

Càceres C, Giménez-Bonafé P, Ribes E, Wouters-Tyrou D, Martinage A, Kouach M, Sautière P, Muller S, Palau J, Subirana JA, Cornudella L, Chiva M. 1999. DNA-interacting proteins in the spermiogenesis of the mollusc *Murex brandaris*. J Biol Chem 274:649–656.

Càceres C, Gimenez-Bonafe P, Zamora MJ, Ribes E, Saperas N, Kasinsky HE, Chiva M. 2000. Protamines in archaeogastropod and caenogastropod molluscs: An example of a radical evolutionary change in a protein model. Trends Comp Biochem Physiol 7:75–82.

Cahn JW. 1965. Phase separation by spinodal decomposition in isotropic systems. J Chem Phys 42:93–99.

Cahn JW, Charles RJ. 1965. The initial stages of phase separation in glasses. Phys Chem Glasses 6:181–191.

Chevaillier P. 1970. Le noyau du spermatozöide et son évolution au cours de la spermiogenèse. In: Baccetti B, editor. Comparative spermatology, Vol. 5. New York: Academic Press. pp 499–514.

Eirín-López JM, Frehlick LJ, Chiva M, Saperas N, Ausió J. 2008. The sperm proteins from amphioxus mirror its basal position among chordates and redefine the origin of vertebrate protamines. Mol Biol Evol 25:1705–1713.

Evans DF, Wennerstrom H. 1999. The colloidal domain: Where physics, chemistry, biology and technology meet. 2nd edition. New York: Wiley-VCH. p 632.

Gallardo CS, Garrido OA. 1989. Spermiogenesis and sperm morphology in the marine gastropod *Nucella crassilabrum* with an account of morphometric patterns of spermatozoa variation in the family Muricidae. Inv Reprod Dev 15:163–170.

Giberson RT, Demaree RS, Jr. 1999. Microwave processing techniques for electron microscopy: A four-hour protocol. Methods Mol Biol 117:145–158.

Gunton JD, Droz M. 1983. Introduction to the theory of metastable and unstable states. Lecture Notes in Physics, No. 183. Berlin: Springer-Verlag. p 140.

Harrison LG. 1993. Kinetic theory of living pattern. UK: Cambridge University Press. p 354.

Harrison LG, Kasinsky HE, Ribes E, Chiva M. 2005. Possible mechanisms for early and intermediate stages of sperm chromatin condensation patterning involving phase separation dynamics. J Exp Zool 303A:76–92.

Jantzen CMF, Herman H. 1978. Spinodal decomposition: Phase diagram representation and occurrence. In: Alper AM, editor. Phase diagrams: Materials science and technology, Vol. 5. New York: Academic Press. pp 127–184.

Jaramillo R, Garrido O, Jorquera B. 1986. Ultrastructural analysis of spermiogenesis and sperm morphology in *Chorus giganteus* (Lesson, 1829) (Prosobranchia: Muricidae). Veliger 29:217–225.

Jones RAJ. 2002. Soft condensed matter. UK: Oxford University Press. p 19.

Kurtz K, Martinez-Soler F, Ausió J, Chiva M. 2007. Acetylaton of histone H4 in complex structural transitions of spermiogenic chromatin. J Cell Biochem 102:1432–1441.

Longo FJ, Anderson E. 1969. Spermiogenesis in the surf clam *Spisula solidissima* with special reference to the formation of the acrosomal vesicle. J Ultrastruct Res 27:435–443.

Longo FJ, Dornfeld EJ. 1967. The fine structure of spermatid differentiation in the mussel, *Mytilus edulis*. J Ultrastruct Res 20:462–480.

McDonald K. 1999. High-pressure freezing for preservation of high resolution for fine structure and antigenicity for immunolabeling. Methods Mol Biol 117:77–97.

McEwan BF, Hsieh C-E, Mattheyses AL, Rieder CL. 1998. A new look at kinetochore structure in vertebrate somatic cells using high-pressure freezing and freeze substitution. Chromosoma 107:366–375.

Mogensen C, Carlos S, Ausió J. 1991. Microheterogeneity and interspecific variability of the nuclear sperm proteins from *Mytilus*. FEBS Lett 282:273–276.

Muller-Reichert T, Hohenberg H, O'Toole ET, McDonald K. 2003. Cryoimmobilization and three-dimensional visualization of *C. elegans* ultrastructure. J Microsc 212(Pt 1):71–80.

Oki K, Sagana H, Eguchi T. 1977. Separation and domain structure of phase in Fe-A1 alloys. J Phys C7:414–417.

Pechenik JA. 2005. Biology of the invertebrates. 5th edition. Boston: McGraw Hill. p 590.

Raspaud E, Olivera de la Cruz M, Sikorav J-L, Livolant F. 1998. Precipitation of DNA by polyamines: A polyelectrolyte behavior. Biophys J 74:381–393.

Rehder HA. 1981. The Audubon Society field guide to North American seashells. New York: Knopf. p 894.

Ribes E, Sanchez De Romero LD, Kasinsky HE, Del Valle L, Giménez-Bonafé P, Chiva M. 2001. Chromatin reorganization during spermiogenesis of the mollusc *Thais hemostoma* (Muricidae): Implications for sperm nuclear morphogenesis in caenogastropods. J Exp Zool 289:304–316.

Ruppert EE, Barnes RD. 1994. Invertebrate zoology. 6th edition. Forth Worth, TX: Saunders College. p 1056.

Turing AM. 1952. The chemical basis of morphogenesis. Philos Trans R Soc Lond B 237:37–72.

Walker MH. 1970. Some unusual features of the sperm of *Nucella lapillus* (L.). In: Baccetti B, editor. Spermatologia comparata. Roma: Academia Nazionale dei Lincei. pp 383–391.

Walker MH, MacGregor HC. 1968. Spermatogenesis and the structure of the mature sperm of *Nucella lapillus* (L.). J Cell Sci 3:95–104.

Wang X, Ausió J. 2001. Histones are the major chromosomal protein components of the sperm of the nemerteans *Cerebratulus californiensis* and *Cerebratulus lacteus*. J Exp Zool 290:431–436.